



HAL
open science

On the Identification and Validation of an Anisotropic Damage Model Using Full-field Measurements

Mouli Ben Azzouna, Jean-Noël Périé, Jean-Mathieu Guimard, François Hild, Stéphane Roux

► **To cite this version:**

Mouli Ben Azzouna, Jean-Noël Périé, Jean-Mathieu Guimard, François Hild, Stéphane Roux. On the Identification and Validation of an Anisotropic Damage Model Using Full-field Measurements. International Journal of Damage Mechanics, 2011, 20, pp.1130-1150. 10.1177/1056789510395555 . hal-00947496

HAL Id: hal-00947496

<https://hal.science/hal-00947496>

Submitted on 18 Feb 2014

HAL is a multi-disciplinary open access archive for the deposit and dissemination of scientific research documents, whether they are published or not. The documents may come from teaching and research institutions in France or abroad, or from public or private research centers.

L'archive ouverte pluridisciplinaire **HAL**, est destinée au dépôt et à la diffusion de documents scientifiques de niveau recherche, publiés ou non, émanant des établissements d'enseignement et de recherche français ou étrangers, des laboratoires publics ou privés.

Submitted to the *International Journal of Damage Mechanics*

Revised version

Special issue on *Multiscale Modeling of Ductile and Brittle Damage in Solids:*

Recent Progresses and New Trends (Guest editors: C. Dascalu, D. Kondo)

**On the identification and validation
of an anisotropic damage model
by using full-field measurements**

by

Mouldi BEN AZZOUNA,¹ Jean-Noël PÉRIÉ,^{1,3} Jean-Mathieu GUIMARD,²

François HILD^{1,*} and Stéphane ROUX¹

¹LMT, ENS Cachan / CNRS / UPMC / PRES UniverSud Paris

61 avenue du Président Wilson, F-94235 Cachan Cedex, France

²EADS – France, Innovation Works

12 rue Pasteur, BP 76, 92152 Suresnes Cedex, France

³now at Université de Toulouse; INSA, UPS, Mines Albi, ISAE

Institut Clément Ader (ICA), 133 avenue de Rangueil, F-31077 Toulouse, France

*Corresponding author. Fax: +33 1 47 40 22 40, Email: hild@lmt.ens-cachan.fr

On the identification and validation of an anisotropic damage model by using full-field measurements

Mouldi BEN AZZOUNA, Jean-Noël PÉRIÉ, Jean-Mathieu GUIMARD,

François HILD and Stéphane ROUX

Abstract: Two different mechanical tests are performed on a laminated composite coupon to induce an anisotropic damage affecting essentially shear modulus softening. The first test is a uniaxial tension loading on a straight coupon, which is used to evaluate the damage law using a conventional approach, while the second contains a notch that enhances dramatically the strain (and hence damage) heterogeneity. A global Digital Image Correlation approach is used to quantify the kinematic fields all along the loading path of the second experiment. Displacement fields are hence evaluated based on a finite-element type discretization. A further exploitation based on the reconditioned equilibrium gap method (and without any further information) gives access to a quantitative measurement of the damage law. The latter approach makes use of a finite-element model based on the very same mesh and element shape function. This full-field based identification method compares very well with traditional techniques, up to the stage where macroscopic localization prevents their subsequent exploitations. Moreover, it is shown that neither the type of mechanical test, nor the discretization of the displacement field, affects the identification of the damage law.

Keywords: Anisotropic damage law, Composite material, Digital Image Correlation, Equilibrium Gap Method, Identification.

1. Introduction

The intensive use of composite materials in the field of aeronautic structures challenges industry on its ability to predict accurately through numerical simulations the behavior of specimens and structures up to failure. In the framework of the VULCOMP project aiming at assessing and quantifying carbon fiber reinforced plastics (CFRP) damage laws (Ladevèze and Le Dantec 1992) in the dynamic loading range, the present work is a first step that proposes an alternative strategy geared towards robust identification of the behavior of a composite ply model by means of a non-conventional test and full field measurements.

The identification of the parameters of anisotropic damage laws involved in CDM models (Voyadjis et al. 1998; Allix and Hild 2002) is usually either performed by resorting to elementary tests on coupons with numerous unloading / loading cycles (e.g., from unidirectional composites (Barbero and Lonetti 2002) or from tensile tests on various stacking sequences (Ladevèze and Le Dantec 1992; Halm et al. 2002; Payan and Hochard 2002; Camanho et al. 2007)) or on notched samples (e.g., shear test on the so-called Iosipescu geometry (Iosipescu 1967; Dickson et al. 1995)). In the first case, central strain gauges are used in addition to a load measurement to retrieve stress-strain relationships at the ply level by using the classical laminate theory. It assumes a uniform strain field up to failure, which is a strong hypothesis that neglects strain and damage localization. In the case of Iosipescu's experiment, uniform strain distributions are assumed in the ligament, even though this is only a first order approximation (Burr et al. 1997). When more complex geometries are considered, or when only corrupted measurements are recorded (e.g. in dynamic loadings), inverse procedures are needed to tune material parameters (Andrieux and Ben Abda 1993; Rota 1994; Allix et al. 2005; Lecompte et al. 2007; Avril et al. 2008). For all these methods, the identification task results in the resolution of an ill-posed problem with constraints given by

trusted experimental data. Up to now, only piecewise global data were used in these methods. Conversely, Chalal *et al.* (2004) resorted to the virtual fields method to determine the parameters of a linear relationship between the damage parameter and the local shear strain. More recently, Lubineau (2009) proposed an iterative FE procedure by means of a filtering technique. It is based on building new field variables (based on simple operations and linear combinations of longitudinal and transverse strain fields) that are more sensitive to each parameter and in each local area.

An alternative route to the previous approaches is given by the equilibrium gap method that aims at identifying fields of elastic contrasts (Claire *et al.* 2002; 2004), which may be reinterpreted *a posteriori* in terms of a damage field (Claire *et al.* 2007; Crouzeix *et al.* 2009). More recently, it was shown that the same type of formalism can be used to directly identify the parameters of the damage law in the case of an isotropic (Roux and Hild 2008) and anisotropic (Périé *et al.* 2009) description of damage. The latter will be used herein to analyze another experiment (here a notched sample to create a heterogeneous strain field), and will be compared to results obtained by analyzing a tensile test on a coupon as an independent validation of the whole procedure. In the present case the studied composite is layered as opposed to the previously studied materials (Roux and Hild 2008; Périé *et al.* 2009)

In the present paper, a notched sample will be used to identify the parameters of a damage law. In Section 2, the experimental conditions are described, and first analyses of kinematic data extracted from displacement measurements thanks to digital image correlation are presented. The identification procedure, namely, the equilibrium gap method is briefly summarized in Section 3, and applied to analyze the experiments on the notched sample in Section 4. The identified damage law is finally compared with that obtained by following a classical approach on a coupon specimen for validation purposes.

2. Description of the experiments

In the work of Périé *et al.* (2009), it has been shown that the Equilibrium Gap method is more powerful when one considers full-field measurements of experimental configurations that undergo non-uniform damage states (and therefore heterogeneous strain fields). Non-uniform fields enable for the activation of a large range of strain distributions at each loading step, whereas a uniform-like test requires the use of many loading steps to reach the same range. To validate this hypothesis, the identified damage law obtained in the analysis of a tensile test on a notched sample is compared with that observed in a classical $[\pm 45]_{\text{ns}}$ tensile test on a coupon (ASTM 1994), see Figure 1.

In the present work, the idea is to enforce geometrically the heterogeneity of strain fields. Consequently, the classical $[\pm 45]_{\text{ns}}$ tensile test on coupons was modified by adding a lateral notch on the specimen. Each layer of the composite is made of unidirectionally aligned carbon fibers (average diameter: 7 μm , volume fraction: 60 %) in a thermoset matrix. The test has been performed on a tension / compression testing machine quasi-statically (stroke rate: 0.5 mm/min) with unloading / loading steps up to final failure of the specimen (Figure 2). The grips were aligned prior to the experiments as usually performed. However, no additional care was taken since the actual boundary conditions are measured for the region of interest by digital image correlation. One face was covered with a random pattern (created by spraying black and white paint). Images are recorded with a digital camera up to failure. The later occurs for a tensile load of about 7500 N (Figure 3). Final failure follows the 45° directions, *i.e.*, the fiber directions.

Thanks to the recorded pictures (at each 500 N step), displacement fields of the prepared face can be measured for each loading steps (Figure 3) by resorting to digital image correlation or DIC (Sutton *et al.* 2009). In the present case, a global correlation algorithm is used (Besnard *et al.* 2006). It allows for the extraction of continuous displacement fields

associated with a finite-element discretization. Four-noded elements are considered with a bilinear interpolation of the displacements in each element. The spatial resolution of the displacement measurement is directly given by the element size. Two element sizes are considered, namely 12 and 34 pixels. These two sizes are considered to analyze the mesh sensitivity of the identified damage law, which is a concern when damage computations are performed. The displacement maps shown in Figure 4 for the two discretizations at the maximum load level are similar. The corresponding strain fields are estimated by computing the average value in each finite element (Figure 5). The spatial resolution of the strains is thus equal to the element size ℓ . There is a more pronounced difference in terms of spatial description of the strain fields when comparing the results obtained for the two discretizations (Figure 5). This is due to the localization of the strains in the vicinity of the highly damaged (V-shaped) zones.

The chosen element sizes lead to a standard displacement uncertainty of the order of 1.5 and 0.3 centipixel, respectively, and a standard strain uncertainty of the order of 10^{-3} and 10^{-4} , respectively. These results are obtained with an *a priori* analysis (Besnard et al. 2006) that consists in prescribing uniform sub-pixel displacements ranging from 0 to 1 pixel, with an 0.1-pixel increment. The root mean square of the measured displacement is estimated for each prescribed value, subsequently averaged over the whole analysis, and referred to as the standard displacement uncertainty σ_u . The strain field is then calculated and the corresponding standard strain uncertainty σ_ε is evaluated by following the same procedure as for the displacements. The results of the analysis are shown in Figure 6. A single power law interpolation of $\sigma_u = A / \ell^\alpha$ and $\ell\sigma_\varepsilon = B / \ell^\alpha$, with $\alpha = 1.7$ and $B / A = 2.3$ describes well the results up to element sizes of the order of 40 pixels. Last, it is to be noted that non-uniform fields are present at each step and localized in the vicinity of the initial notch (Figure 2) that

may induce interpolation errors if the displacement field is not sufficiently discretized, especially in terms of strain fields (Figure 5).

This result is confirmed by the equivalent shear strain maps plotted for the classical tensile test and for the test on a notched sample (Figure 7). Heterogeneity becomes significant only at the final stages of the loading. For comparison purposes, the distributions of equivalent strains in the coupon and notched sample (with two different discretizations) are shown in Figure 8. In the classical test, the range of strains is not as high as that observed in the notched sample. This is especially true for the last load levels, for which the range is quasi-constant for each cycle of the classical test. The strain histograms of the notched sample using two discretizations are also different, thereby illustrating the effect of the spatial resolution of the measurement technique in the presence of heterogeneous strain fields. In the following, an identification technique making use of the FE measured displacement fields will be utilized in the framework of the equilibrium gap method.

3. Equilibrium Gap Method

3.1 Damage model

In the following, a $[0/90]_{ns}$ stacking sequence is considered (a simple rotation leads to the actual configuration studied, see Figure 1). The composite behavior is described at the macroscopic scale for the sake of simplicity (delamination degradation does not occur in this configuration which means that the mesoscopic and macroscopic scales are similar), and only in-plane stress components are considered. It is assumed that the dominant degradation mechanism is related to shear damage modeled by a single variable D . Gibbs' free enthalpy Ψ of the composite then reads

$$\Psi = \frac{1}{2} \left[\frac{\sigma_{11}^2}{E_1} - \frac{\nu_{12}}{E_1} \sigma_{11} \sigma_{22} + \frac{\sigma_{22}^2}{E_2} + \frac{\sigma_{12}^2}{G_{12}(1-D)} \right] \quad (1)$$

where σ_{11} , σ_{22} , σ_{12} are the in-plane stress components expressed in the material frame (1, 2). The elastic properties are E_1 and E_2 (Young's moduli along the fiber directions), ν_{12} (Poisson's ratio), and G_{12} (in-plane shear modulus). The in-plane strain components are expressed as

$$\begin{aligned}\varepsilon_{11} &= \frac{\partial \Psi}{\partial \sigma_{11}} = \frac{\sigma_{11}}{E_1} - \frac{\nu_{12}}{E_1} \sigma_{22} \\ \varepsilon_{22} &= \frac{\partial \Psi}{\partial \sigma_{22}} = \frac{\sigma_{22}}{E_2} - \frac{\nu_{12}}{E_1} \sigma_{11} \\ 2\varepsilon_{12} &= \frac{\partial \Psi}{\partial \sigma_{12}} = \frac{\sigma_{12}}{G_{12}(1-D)}\end{aligned}\quad (2)$$

and the thermodynamic force Y associated with the damage variable D becomes

$$Y = \frac{\partial \Psi}{\partial D} = \frac{\sigma_{12}^2}{2G_{12}(1-D)^2} = 2G_{12}\varepsilon_{12}^2 \quad (3)$$

Equation (3) shows that the thermodynamic force Y is directly related to the shear strains, which are accessible thanks to kinematic measurements. The growth of the damage variable D is assumed to be driven by Y (Herakovich et al. 2000). It is worth noting that other driving forces have been proposed for fabric tapes (Hochard et al. 2007) but for the UD laminate studied herein, this simple expression is in good accordance with microscopic observations (Kellas et al. 1993). Consequently, the damage variable D becomes a function of an equivalent strain $\hat{\varepsilon}_{eq}$ such that

$$D = \sum_k c_k \varphi_k(\hat{\varepsilon}_{eq}) \quad \text{with} \quad \hat{\varepsilon}_{eq}(t) = \max_{0 \leq \tau \leq t} |\varepsilon_{12}(\tau)| \quad (4)$$

where φ_k are functions to be specified later on, and c_k are the material parameters to be tuned.

In the next section, the equilibrium gap method is summarized to identify the parameters c_k .

3.2 Identification procedure

The identification procedure followed herein consists in prescribing the measured nodal displacements to a finite element model in which the mesh and the kinematic hypotheses are *identical*. When applying displacements to inner nodes on which no external forces are prescribed, nodal forces arise. In a finite element framework, the residual force vector $\{\mathbf{f}_{res}\}$ reads

$$\{\mathbf{f}_{res}\} = [\mathbf{K}(\{\mathbf{D}\})]\{\mathbf{u}_{meas}\} \quad (5)$$

where the stiffness matrix $[\mathbf{K}]$ depends upon the damage vector $\{\mathbf{D}\}$, and $\{\mathbf{u}_{meas}\}$ denotes the measured displacement vector. In the present case, it is assumed that the damage variable is uniform in each considered Q4 element. Therefore, the elementary stiffness matrix $[\mathbf{K}^{el}]$ is affine in D

$$[\mathbf{K}^{el}(D)] = [\mathbf{K}^0] - D[\mathbf{K}^1] \quad (6)$$

where $[\mathbf{K}^0]$ and $[\mathbf{K}^1]$ are dependent upon elastic properties of the undamaged material (here assumed to be known)

$$[\mathbf{K}^0] = \begin{bmatrix} k_{11}^0 & k_{12}^0 & 0 \\ k_{12}^0 & k_{22}^0 & 0 \\ 0 & 0 & k_{33}^0 \end{bmatrix}, \quad [\mathbf{K}^1] = \begin{bmatrix} 0 & 0 & 0 \\ 0 & 0 & 0 \\ 0 & 0 & k_{33}^0 \end{bmatrix} \quad (7)$$

where k_{ij}^0 ($i,j = 1,3$) are dependent upon the elastic properties of the layers. If it is assumed that the damage variable follows the same growth law in the region of interest, Equation (4) provides a *unique* relationship between the damage field $D(\mathbf{x})$ and the corresponding equivalent strain field $\hat{\varepsilon}_{eq}(\mathbf{x})$. The force residuals should be made as small as possible. This is possible by tuning the parameters of the damage law. Minimizing the equilibrium gap E_g

$$E_g = \|\{\mathbf{f}_{res}\}\|^2 \quad (8)$$

is equivalent to minimizing the reconditioned equilibrium gap \tilde{E}_g (Péridé et al. 2009)

$$\tilde{E}_g(c_k) = \sum_i \left(u_i - \sum_k c_k \sum_j S_{ij} \sum_e L_{je}^1 \varphi_k(\hat{\varepsilon}_{eq}^e) \right)^2 \quad (9)$$

where u_i is the i -th component of the measured nodal displacements, L_{ie}^1 the contribution of element e to the nodal force at the internal node i ($L_{ie}^1 = \sum_j K_{ije}^1 u_j$), and S_{ij} the component of the operator $[\mathbf{S}]$ defined by $[\mathbf{S}]\{\mathbf{L}\} = \{\mathbf{u}_{meas}\}$. It is to be emphasized that in spite of the proposed non-linear constitutive damage law, the identification consists in solving a *linear* system in the unknown c_k parameters (minimization of a quadratic functional). The reconditioned functional \tilde{E}_g is much less sensitive than E_g to the short wavelength noise, which is inevitably present in the determination of the displacement field. Hence the proposed formulation is robust, and of very small size (the number of unknowns is typically very small). As already used in previous studies (Roux and Hild 2008; Péridé et al. 2009), functions φ_k are written as

$$\varphi_k(\hat{\varepsilon}_{eq}) = 1 - \exp\left(-\frac{\hat{\varepsilon}_{eq}}{\varepsilon_k}\right) \quad (10)$$

where the values ε_k are considered in the range of experimentally observed equivalent strains, and well separated (typically, $\varepsilon_{k+1} / \varepsilon_k = 2$). When only one parameter c_k is not equal to zero, the classical range $[0;1]$ of a damage variable is automatically satisfied. Equation (4) is a constitutive law *regularization*. It enforces the strong condition that two regions where the equivalent strain is the same will experience an identical damage level. Let us finally note that Equation (4) can be read as a truncated Laplace transform of the damage law.

4. Identification and validation

4.1. Data extraction

In this study, the identification consists in estimating the damage part of all non-linear mechanisms involved in the degradation of composite materials. Since DIC yields displacement fields in the notched sample at each chosen load level (up to failure) with respect to any reference step, there are many possible choices. Classically, the reference picture is that of the initial step for which no load was applied (i.e., at the very beginning of the experiment). However, it is possible to consider the picture corresponding to each unloaded step as the reference, and the next one corresponding to the subsequent maximum load level (see Figure 3). By using the present procedure, it is therefore possible to analyze only the part of the behavior corresponding to the damage state (disregarding plastic-like components).

It is to be stressed that the actual experimental boundary conditions (even if imperfect) are taken into account from the Dirichlet conditions to be used in the identification procedure. Hence, spurious rotations or torques that are likely to appear for the most damaged states are taken into account, making this identification procedure much more tolerant to imperfections in the loading conditions or natural breakdown of symmetries.

4.2. Identification results

By using the damage law (4), the identification results yield the unknowns c_k for chosen ε_k values (Table 1). The quality of the identification is first assessed globally by computing the standard deviation of the displacement difference related to that of the measured displacement. This indicator is denoted by ρ_u . Second, the field of displacement differences allows for a local analysis of the identification result.

Table 1: Identification results for the two considered discretizations.

ε_k	c_k (12 pixels)	c_k (34 pixels)
0.042 max range $\varepsilon_k = 0.016 \times [1;2;4;8]$	Best solution obtained for [1.0;0;0;0]	
0.033 max range $\varepsilon_k = 0.012 \times [1;2;4;8]$		Best solution obtained for [1.0;0;0;0]
Displacement residual ρ_u	Image 5 to 14: [11.3 to 3.7] %	Image 5 to 14: [6.4 to 5.6] %

From the measurement of the equivalent strain map and the determination of the parameters of the damage law, it is possible to construct the damage maps for each of the analyzed load levels (Figure 9). From Figures 7 and 8, it is to be expected that the notch enables for the exploration of higher strain levels prior to failure, and consequently for the identification of higher levels of damage. For the last considered cycle (#14), a localized damage pattern is observed with a value of d_{I2} approaching 1. This is in good accordance with the experimental failure pattern observed in Figure 2. For the two discretizations (12-pixel and 34-pixel sizes), the best solution is obtained with only one parameter ε_k for which c_k is therefore close to 1. This result shows that the identified damage law given by Equation (4) is similar for the two discretizations.

The whole identification procedure interpreted in terms of a constitutive law is *a priori* only valid prior to localization. Beyond localization onset, the DIC analysis may smooth out sharp gradients. Similarly, numerical simulations are inadequate as they become mesh-

dependent. However, here both DIC and simulation are performed with the *same* mesh, and hence they are expected to share these flaws, and yet they can be compared. At this point, the determination of the damage law is not unique. However, because of the very few parameters introduced to describe it, no indeterminacy appears, and the comparison remains quite satisfactory.

4.3. Validations

A first way of validating the identification results is to compare the computed displacement field using the damage law that was identified with the measured displacement field, and then estimate the displacement residuals (Table 1). Figure 10 shows the three maps corresponding to the two displacement components for cycles #4 and #14. A very good agreement is observed. The relative displacement residual ρ_u is about 3.7 % for 12-pixel elements and 5.6% for 34-pixel elements for the final cycle, which leads to a low sensitivity to the uncertainty level (Figure 6) associated with DIC. The fact that ρ_u is smaller for 12-pixel elements than the value for 34-pixel elements indicates that the discretization with 12-pixel elements better captures the damage pattern.

Another way of validation is given by the damage law itself. The latter is compared with that obtained by following the classical identification procedure (Ladevèze and Le Dantec 1992). In the latter, only a single longitudinal strain level (Figure 1) is available per unloading / loading cycle. From 10 to 15 points are generally accessible. For example, Figure 11 shows the result from the analysis for which only 5 points lie above the damage threshold. For the present approach, the same results are shown in Figure 11. Numerous identification points are available thanks to full-field data. It is also to be noted that the present approach allows for the identification of damage levels greater than 0.4, level at which the global method stops because of failure that occurs suddenly.

In the range over which the two results can be compared, there is a good agreement, thereby validating the approach followed herein. It is to be remembered that the damage functions (10) do not incorporate a threshold parameter. This is the main difference between the two results. However, it is believed that this value is difficult to capture with fine meshes for which the measurement uncertainty is not sufficiently small.

5. Summary and Outlook

This paper proposes a robust damage law identification based on full-field measurements and using a non-conventional test. It was validated against classical procedures. It is to be emphasized that the power of the proposed method comes from the exploitation of heterogeneous tests. Each element can be seen as an elementary test on its own, but in addition the equilibrium condition provides additional information on stresses being transferred from one element to its neighbors. Even if this information is relative (in the absence of external load measurements), it provides a very severe constraint on the estimation of the local damage state. The ill-posed character of the identification procedure as an inverse problem is tamed by using a law formulation rather than a stiffness field measurement. Moreover, a reconditioned method allows for the construction of a residual based on displacement fields (as can be seen from dimensional analysis) rather than on their second derivatives (residual body forces). This approach dampened the noise sensitivity of the searched material properties.

The validation is performed on the very same mesh as the measurement itself. The fact that two mesh sizes have led to the same growth law is a validation on the mesh insensitivity prior to localization. Let us underline that the fact that measured and not assumed boundary conditions are considered makes the identification procedure more realistic.

The present analysis focused only on the damage law identification but the method is currently extended to identify the inelastic (or plastic-like) effects. This is made possible by analyzing the sequence of pictures shot at zero load with respect to the reference picture. The fact that the damage state is already known with the present approach will allow for a decoupled identification procedure.

Acknowledgments

This work was funded by Agence Nationale de la Recherche under the grant ANR-2006-MAPR-0022-01 (VULCOMP Phase 1 Project).

References

- Allix, O., Feissel, P., and Nguyen, H. M. (2005). "Identification strategy in the presence of corrupted measurements." *Eng. Comput.*, 22 (5-6), 487-504.
- Allix, O., and Hild, F. (2002). *Continuum Damage Mechanics of Materials and Structures*. Elsevier, Amsterdam (the Netherlands).
- Andrieux, S., and Ben Abda, A. (1993). "The reciprocity gap: a general concept for flaws identification problems." *Mech. Res. Comm.*, 20 (5), 415-420.
- ASTM (1994). "*D3518 / D3518M Standard test method for in-plane shear response of polymer matrix composite materials by test of a $\pm 45^\circ$ laminate.*" In, ASTM, West Conshohocken, PA (USA)
- Avril, S., Bonnet, M., Bretelle, A.-S., Grédiac, M., Hild, F., Ienny, P., Latourte, F., Lemosse, D., Pagano, S., Pagnacco, E., and Pierron, F. (2008). "Overview of identification methods of mechanical parameters based on full-field measurements." *Exp. Mech.*, 48 (4), 381-402.
- Barbero, E. J., and Lonetti, P. (2002). "An Inelastic Damage Model for Fiber Reinforced Laminates." *J. Comp. Mat.*, 36, 941-962.

- Besnard, G., Hild, F., and Roux, S. (2006). "Finite-element displacement fields analysis from digital images: Application to Portevin-Le Châtelier bands." *Exp. Mech.*, 46, 789-803.
- Burr, A., Hild, F., and Leckie, F. A. (1997). "Continuum Description of Damage in Ceramic-Matrix Composites." *Eur. J. Mech. A/Solids*, 16 (1), 53-78.
- Camanho, P., Maimí, P., and Dávila, C. (2007). "Prediction of size effects in notched laminates using continuum damage mechanics." *Comp. Sci. Tech.*, 67 (13), 2715-2727.
- Chalal, H., Meraghni, F., Pierron, F., and Grédiac, M. (2004). "Direct identification of the damage behaviour of composite materials using the virtual fields method." *Composites: Part A*, 35, 841-848.
- Claire, D., Hild, F., and Roux, S. (2002). "Identification of damage fields using kinematic measurements." *C. R. Mécanique*, 330, 729-734.
- Claire, D., Hild, F., and Roux, S. (2004). "A finite element formulation to identify damage fields: The equilibrium gap method." *Int. J. Num. Meth. Engng.*, 61 (2), 189-208.
- Claire, D., Hild, F., and Roux, S. (2007). "Identification of a Damage Law by Using Full-Field Displacement Measurements." *Int. J. Damage Mech.*, 16 (2), 179-197.
- Crouzeix, L., Périé, J.-N., Collombet, F., and Douchin, B. (2009). "An orthotropic variant of the Equilibrium Gap Method applied to the analysis of a biaxial test on a composite material." *Composites: Part A*, 40 (11), 1732-1740.
- Dickson, T., Munro, M., and Lee, S. (1995). "Selection of an in-plane shear test method based on the shear sensitivity of laminate tensile modulus." *Composites*, 26 (1), 17-24.
- Halm, D., Dragon, A., and Charles, Y. (2002). "A modular damage model for quasi-brittle solids – interaction between initial and induced anisotropy." *Arch. Appl. Mech.*, 72, 498-510.

- Herakovich, C. T., Schroedter, R. D., Gasser, A., and Guitard, L. (2000). "Damage evolution in $[\pm 45]_s$ laminates with fiber rotation." *Comp. Sci. Tech.*, 60 (15), 2781-2789.
- Hochard, C., Lahellec, N., and Bordreuil, C. (2007). "A ply scale non-local fibre rupture criterion for CFRP woven ply laminated structures." *Comp. Struct.*, 80 (3), 321-326.
- Iosipescu, N. (1967). "New Accurate Procedure for Single Shear Testing of Metals." *J. Mater.*, 2, 537-566.
- Kellas, S., Jackson, K. E., and Morton, J. (1993). "Damage and Failure Mechanisms in Scaled Angle-Ply Laminates." *Composite Materials: Fatigue and Fracture*, 4, 257-280.
- Ladevèze, P., and Le Dantec, E. (1992). "Damage modelling of the elementary ply for laminated composites." *Comp. Sci. Tech.*, 43 (3), 257-267.
- Lecompte, D., Smits, A., Sol, H., Vantomme, J., and Hemelrijck, D. V. (2007). "Mixed numerical-experimental technique for orthotropic parameter identification using biaxial tensile tests on cruciform specimens." *Int. J. Solids Struct.*, 44 (5), 1643-1656.
- Lubineau, G. (2009). "A goal-oriented field measurement filtering technique for the identification of material model parameters." *Comput. Mech.*, 44 (5), 591-603.
- Payan, J., and Hochard, C. (2002). "Damage modelling of laminated carbon/epoxy composites under static and fatigue loadings." *Int. J. Fat.*, 24 (2-4), 299-306.
- Périeré, J. N., Leclerc, H., Roux, S., and Hild, F. (2009). "Digital Image Correlation and biaxial test on composite material for anisotropic damage law identification." *Int. J. Solids Struct.*, 46, 2388-2396.
- Rota, L. (1994). "An inverse approach for identification of dynamic constitutive equations." *Proceedings Inverse Problems in Engineering mechanics*, Balkema
- Roux, S., and Hild, F. (2008). "Digital Image Mechanical Identification (DIMI)." *Exp. Mech.*, 48 (4), 495-508.

Sutton, M. A., Orteu, J.-J., and Schreier, H. (2009). *Image correlation for shape, motion and deformation measurements*. Springer.

Voyadjis, G. Z., Ju, J.-W. W., and Chaboche, J.-L. (1998). *Damage Mechanics in Engineering Materials*. Elsevier, Amsterdam (the Netherlands).

Figures

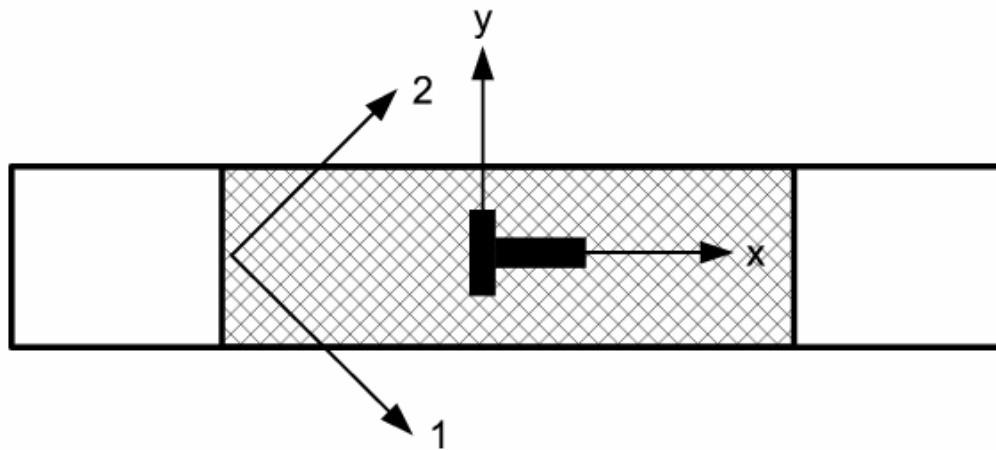


Figure 1: Schematic view of the classical tensile test coupon with longitudinal and transverse strain gauges (in black). In the present case a $\pm 45^\circ$ configuration is depicted.

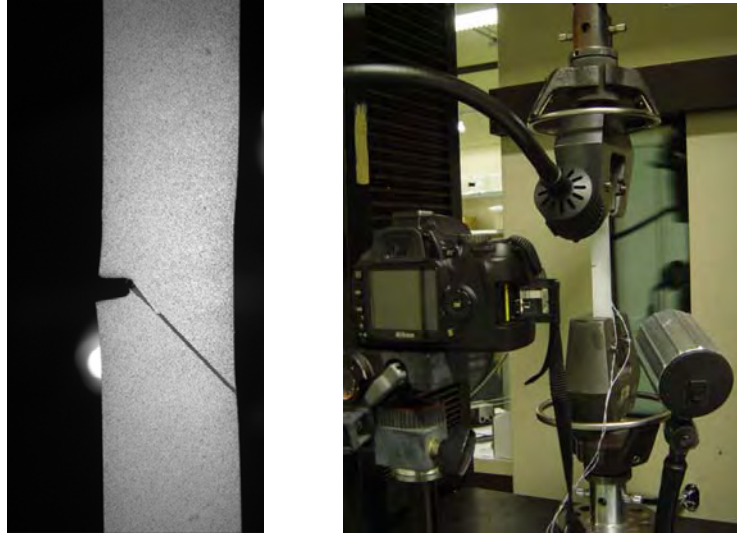


Figure 2: Picture of the prepared surface at failure (left) and experimental set-up (right).

The pixel size corresponds to a physical length scale of 36 μm .

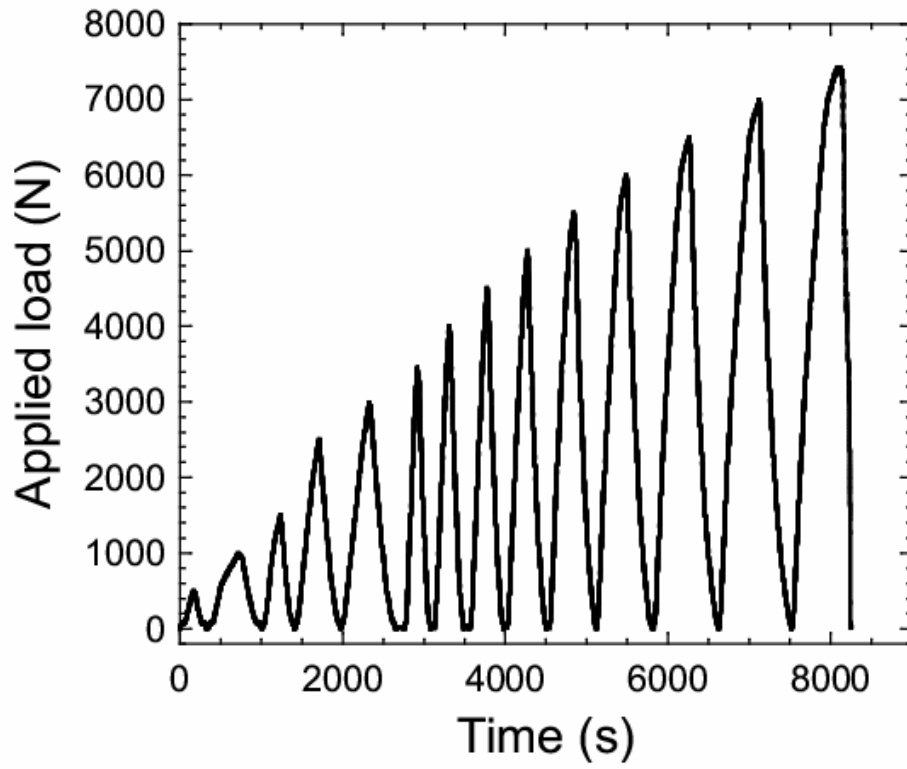


Figure 3: Applied load (N) versus time (s). Each local peak data were used to measure displacement fields by resorting to DIC.

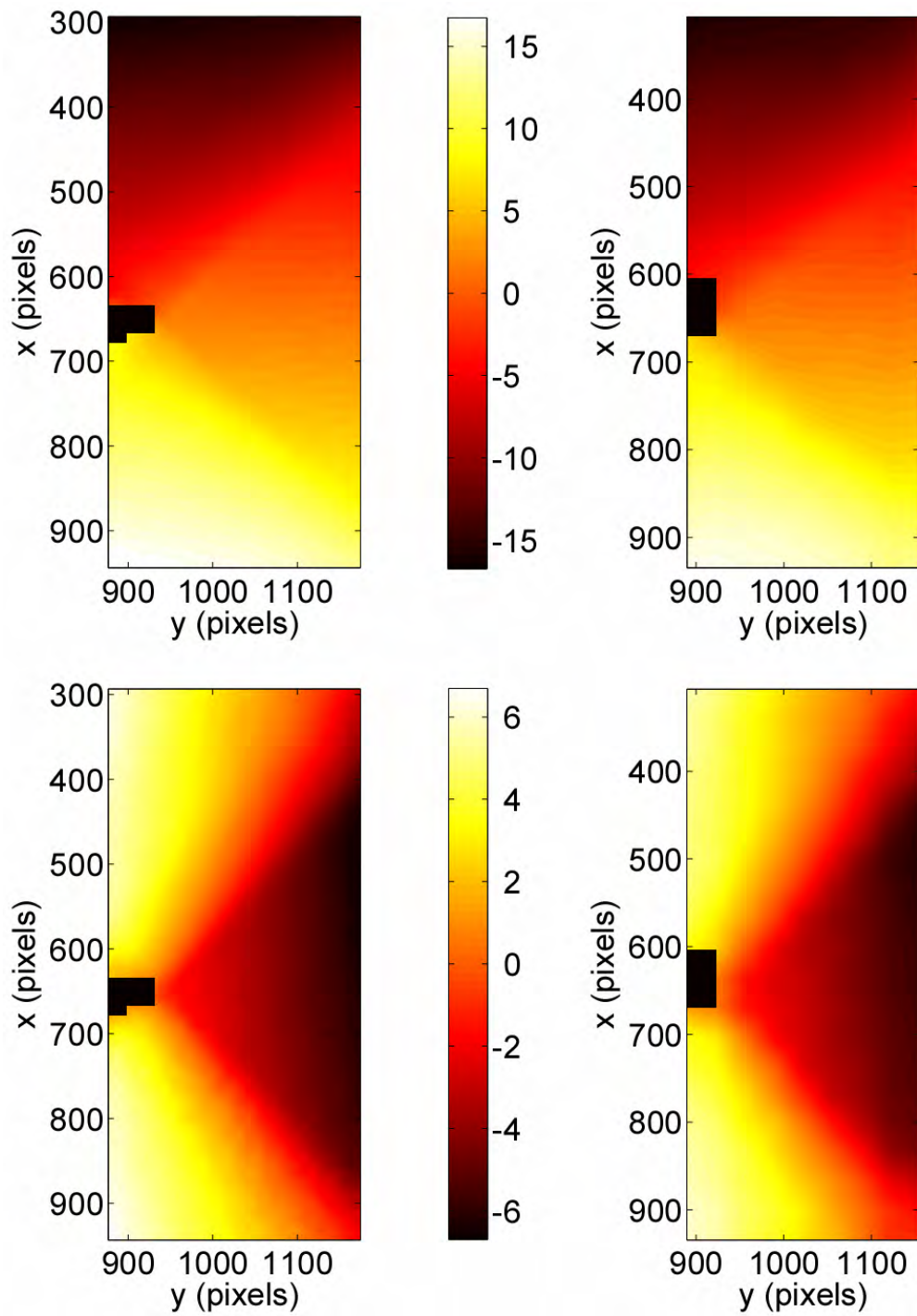


Figure 4: Displacement maps u_x (top) and u_y (bottom) expressed in pixels (1 pixel \leftrightarrow 36 μm) at maximum load of the notched specimen with a 12-pixel (left) and 34-pixel (right) discretization. The rigid body motion was removed.

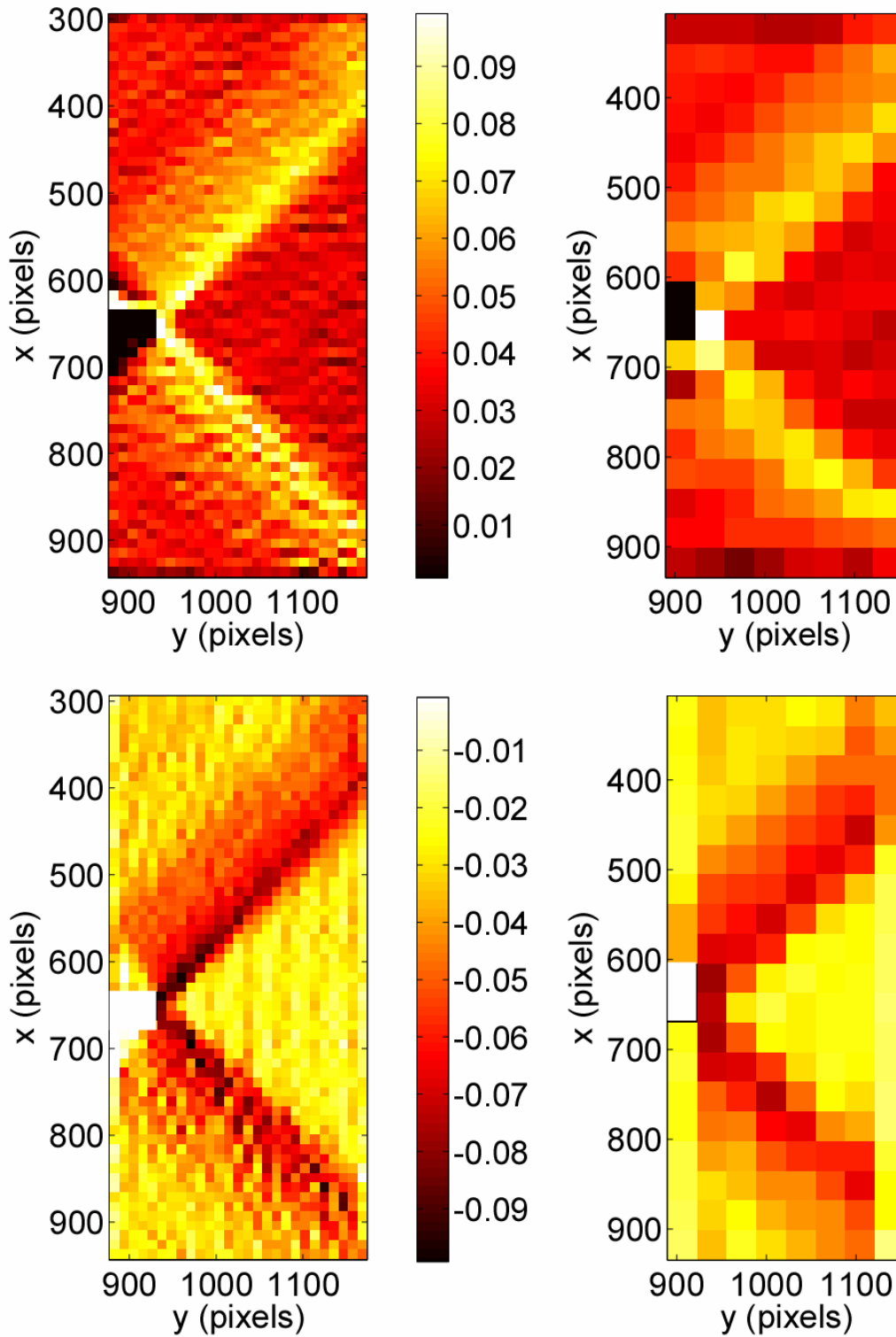


Figure 5: Strain maps ε_{xx} (top) and ε_{yy} (bottom) at last step of the analysis of the notched specimen with a 12-pixel (left) and 34-pixel (right) discretization. Strain localization (along the fiber directions) is clearly visible on both maps of the finer discretization.

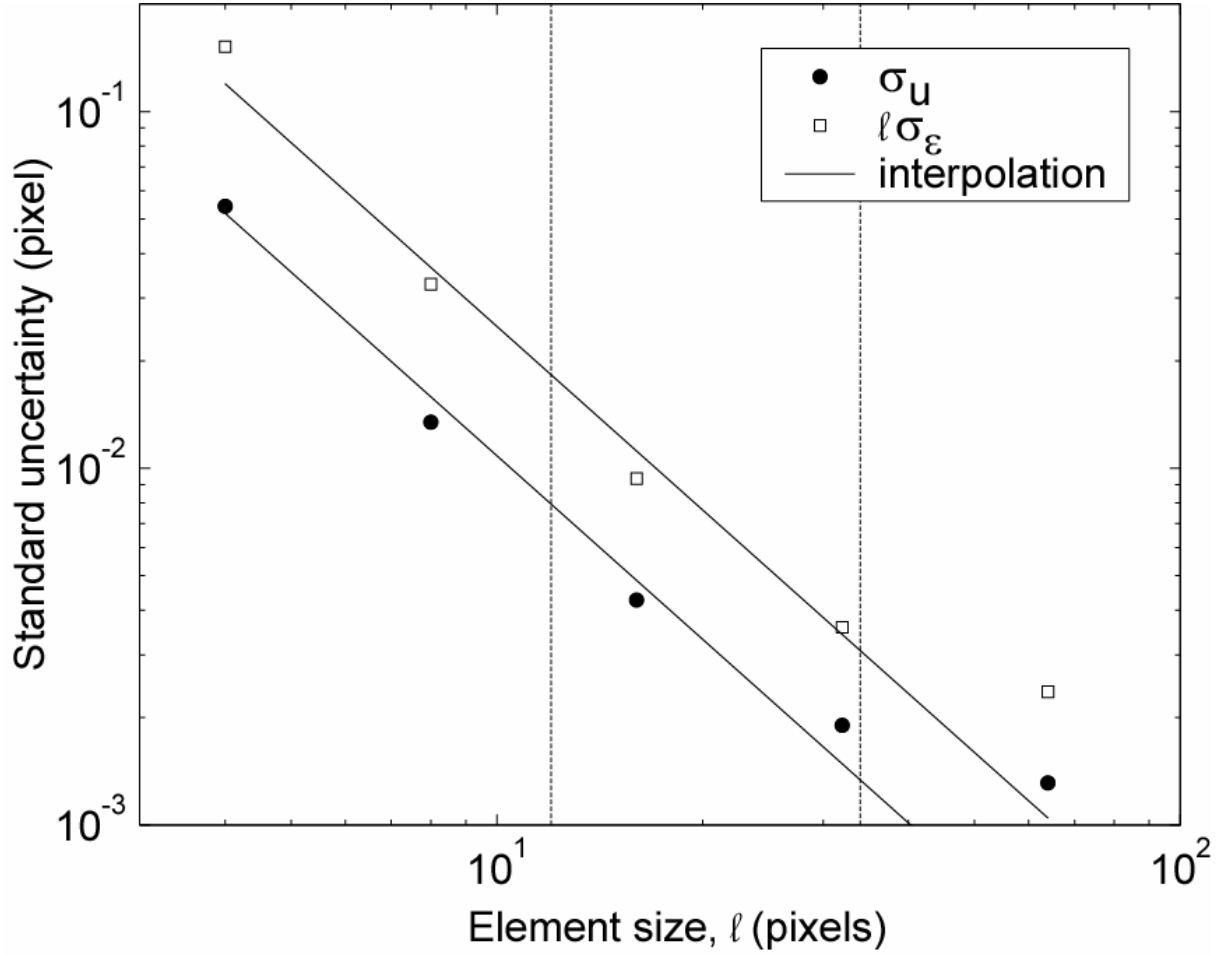


Figure 6: A priori analysis of the standard displacement (σ_u) and strain (σ_ϵ) uncertainties as functions of the element size (ℓ) for the reference picture of the analyzed experiment. The symbols are measurement results and the solid lines correspond to a power law fit.

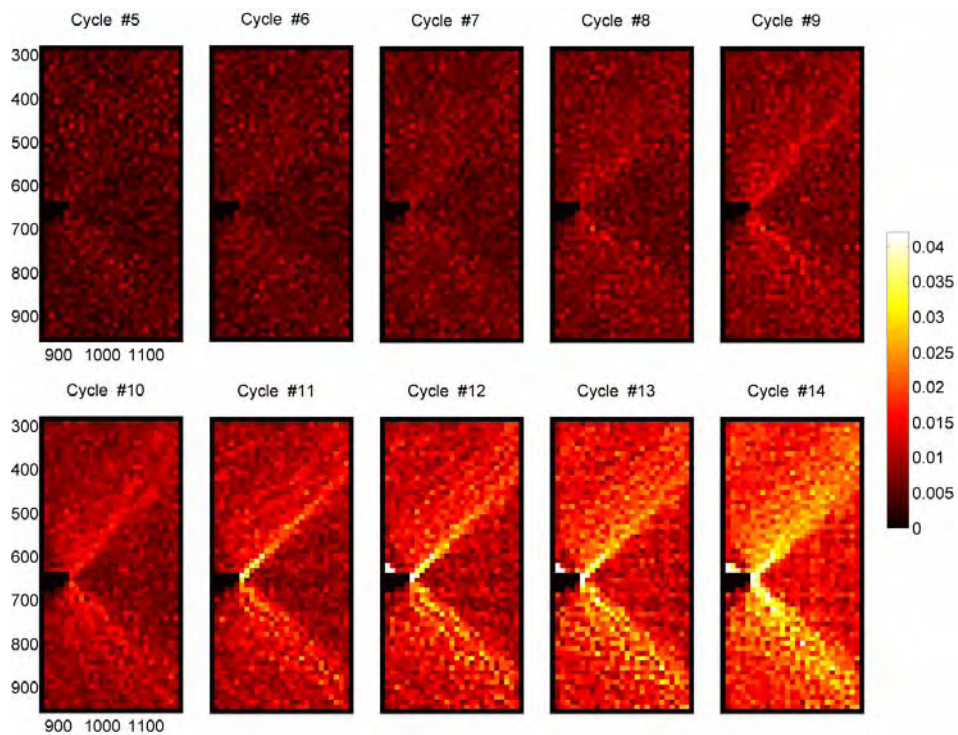
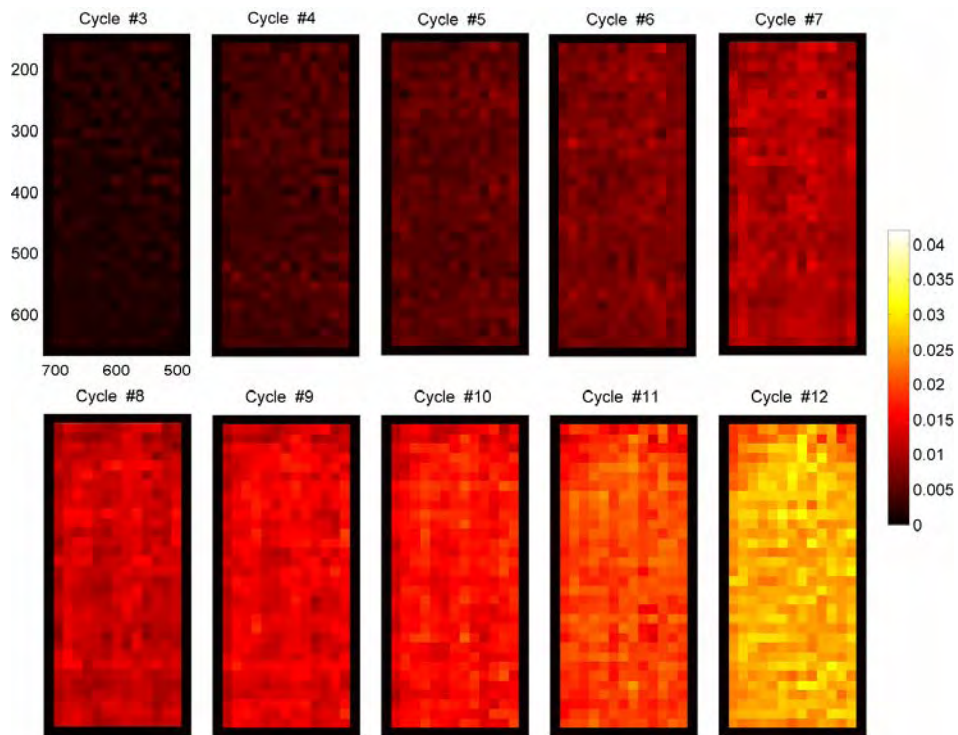


Figure 7: Equivalent (shear) strain maps for each step up to failure in a tensile test for the classical geometry (top: cycles #3 to #12) with a 16-pixel discretization, and for a notched sample (bottom: cycles #5 to #14) with a 12-pixel discretization.

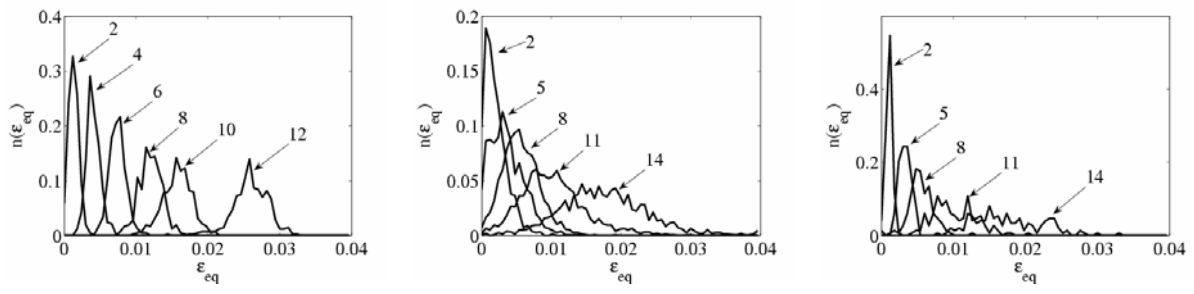


Figure 8: Probability density functions of equivalent strains in the classical geometry with a 16-pixel discretization (left), and in the notched specimen with 12-pixel (middle) and 34-pixel (right) discretizations. Each curve corresponds to one cycle.

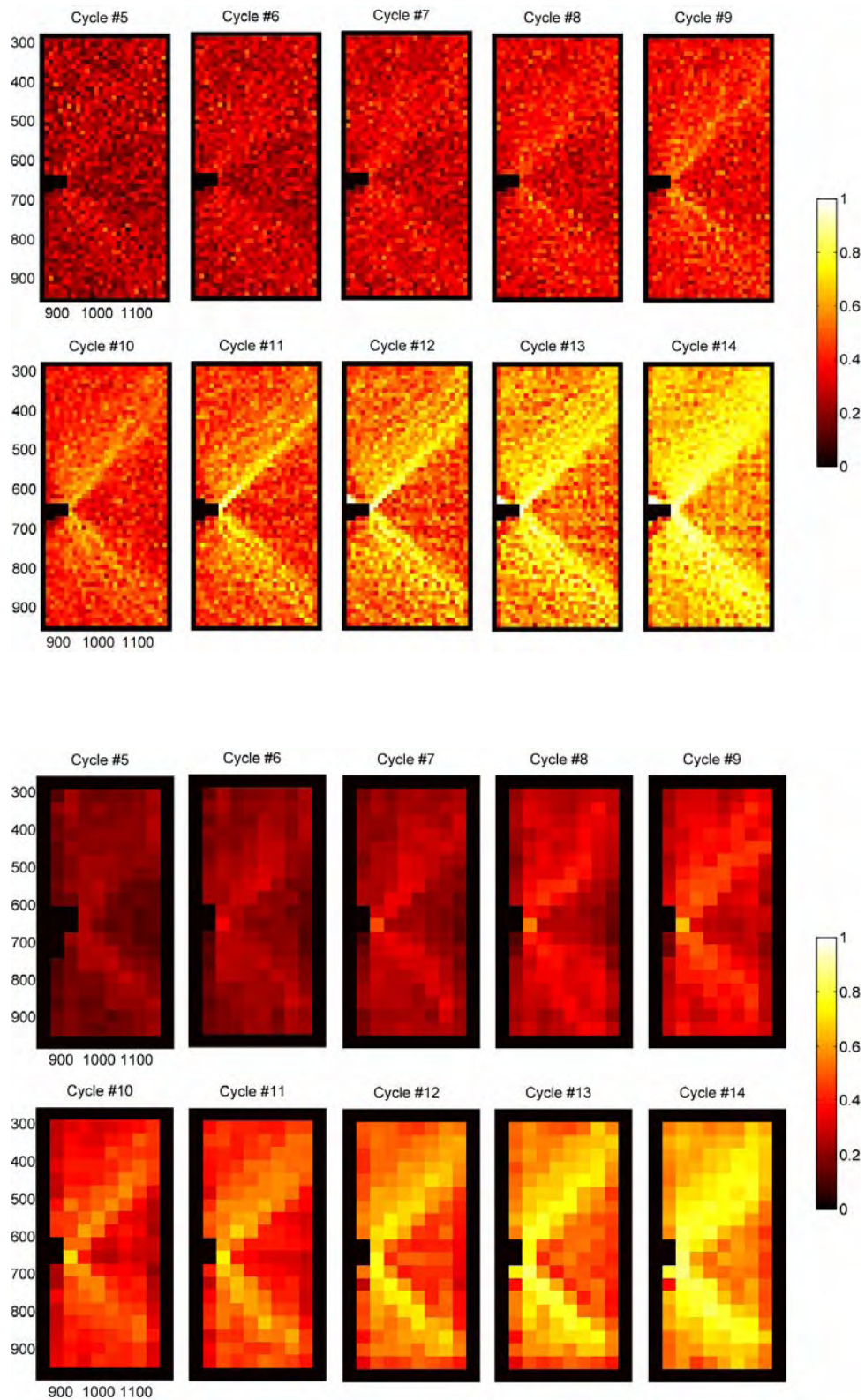


Figure 9: Identified damage maps for each analyzed cycle for two element sizes:

12 pixels (top), and 34 pixels (bottom).

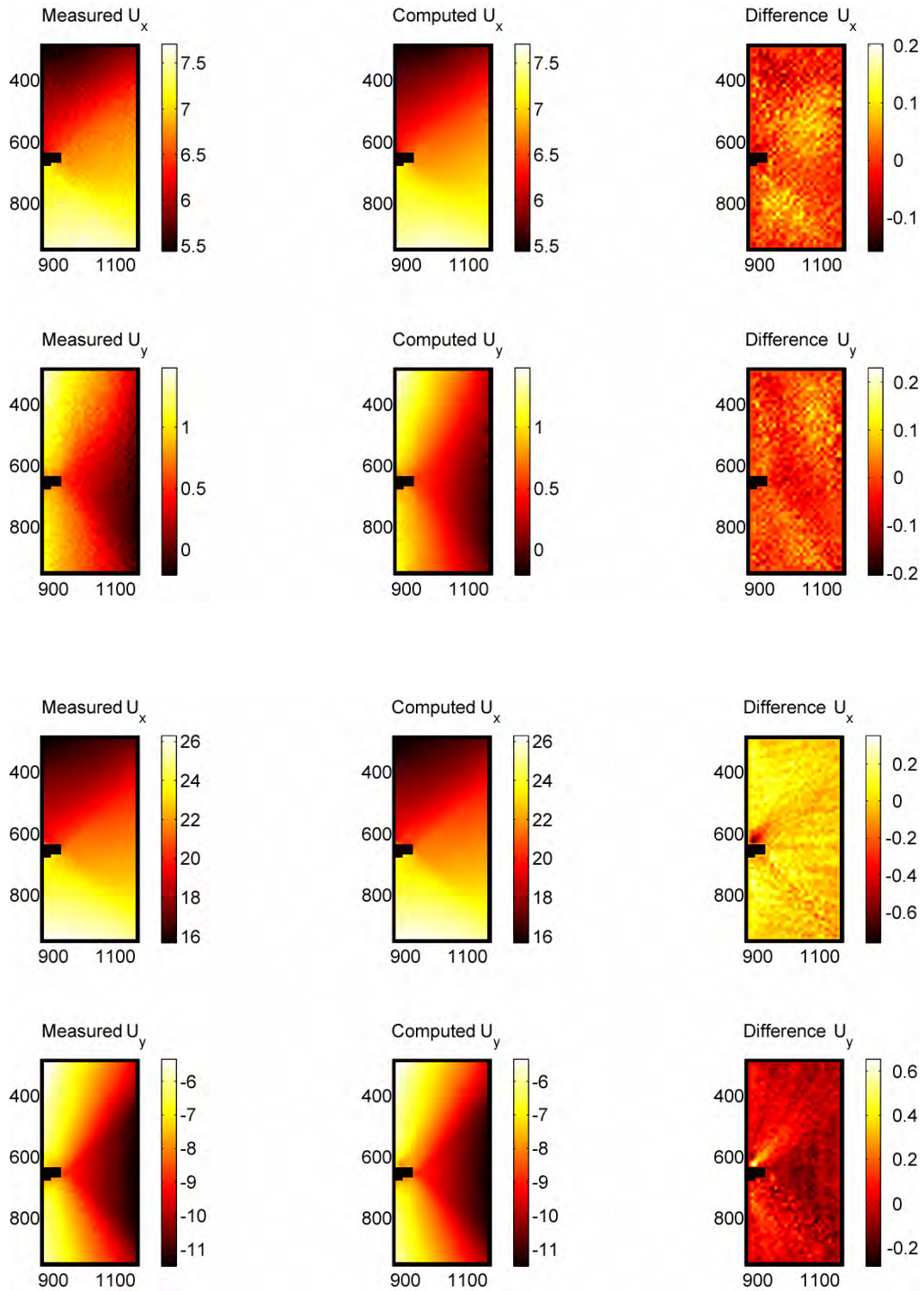


Figure 10: Comparison of the measured and computed displacement fields (top: cycle #4, bottom: cycle #14) for the 12-pixel discretization.

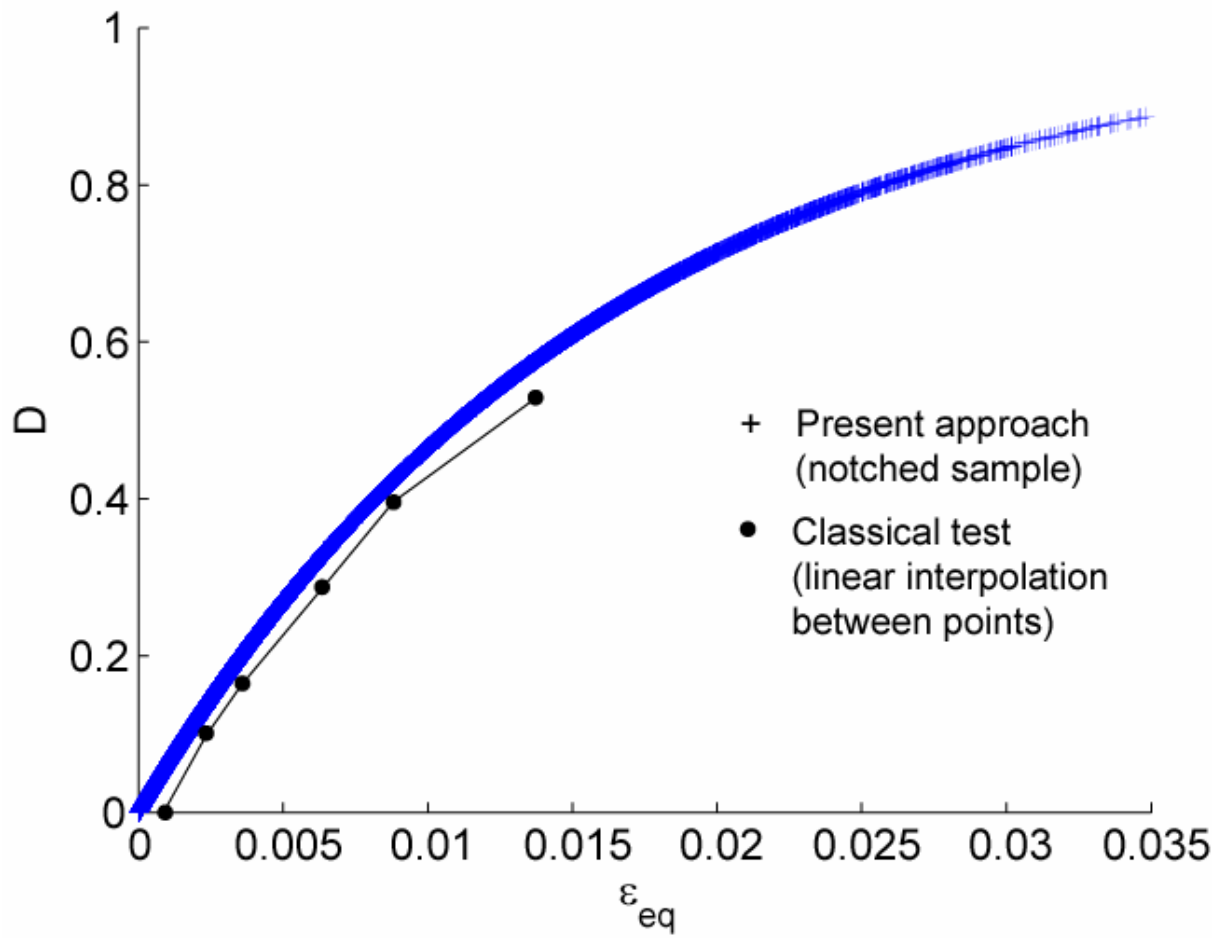


Figure 11: Damage law identified by following the classical approach (few strain data are available) and by resorting to full-field measurements and the equilibrium gap method. Each cross corresponds to a measured strain.